A Numerical Study on the Ability to Measuring the Heat Release Rate, Equivalence Ratio and NO Emission Using Chemiluminescence in Counterflow Premixed Methane Flames

Yushuai Liu[1*], George Vourliotakis[1], Yannis Hardalupas[1], A. M. K. P. Taylor[1]
[1] Department of Mechanical Engineering Imperial College London, United Kingdom

Abstract

Chemiluminescence emission from flames has been implemented to monitor and control heat release rate (HRR), local equivalence ratio (ER) and key pollutant emissions in gas turbine combustors and automotive engines. In the present study, in order to simultaneously simulate the chemiluminescence of OH^*, $CH^*(A)$, C_2^* and CO_2^* (where * denotes the excited state) and to obtain insight on the relation between chemiluminescence, heat release, equivalence ratio and NO emission, numerical studies on 1-D counterflow premixed methane flames were conducted. A new detailed reaction mechanism, incorporating sub-reaction models for excited state OH^*, $CH^*(A)$, C_2^* and CO_2^* radicals was assembled in this study. Three detailed reaction mechanisms available in the literature for C1–C3 hydrocarbons were employed in the current work. Results show that OH^*, $CH^*(A)$ and CO_2^* chemiluminescence can accurately reproduce the heat release rate trend, while the $OH^*/CH^*(A)$ chemiluminescent intensity ratio varies non-monotonically with the equivalence ratio. Further, it is shown that the CO_2^* and C_2^* chemiluminescence can be utilized to indicate the levels of NO emissions. However, the choice of the fuel oxidant chemical mechanism can highly influence the model's ability to predict the behavior of the aforementioned combustion parameters through chemiluminescence simulations.

Introduction

Premixed counterflow flames have been received much attention in the last few decades due to their one dimensional geometry and the fact that they can be used to vary the stretch rate conveniently. Numerous theoretical, experimental and numerical studies have discussed their flow field [1-3], flame speed [4, 5], extinction behaviour [3, 6], flame temperature [7, 8], species distribution [2, 9] and pollutant emission [10-13] as well as chemiluminescence [14-17]. Since chemiluminescence can provide much useful information including heat release rate (HRR) [15, 18-20], equivalence ratio (ER) [15, 16, 21-24] and location of the reaction zone [14, 21, 22, 25, 26], it has been widely used in research and industrial combustor control [19, 27].

So far, several researches have investigated the detailed chemical mechanism of the chemiluminescence of different excited species [20, 28, 29]. Generally, the detailed chemical mechanism is assembled fromthree kinds of reactions, which are formation reactions, collisional quenching reactions and radiative destruction reactions. In the chemiluminescence mechanism, the formation reactions dominate the mole fraction or concentration of excited species in the calculated flames.

For the OH^* molecule's formation, two pathways are accepted, which are the hydrocarbon oxidation pathway (R1) and hydrogen oxidation path way (R2):

$$CH+O_2=OH^*+CO \quad (R1)$$
$$H+O+M=OH^*+M \quad (R2)$$

A comprehensive review on OH^* formation reactions can be found in reference [30]. Although, in hydrocarbon flames, the dominant formation pathway of OH^* is R1 [31], pathway R2 enables the mechanism to predict the OH^* formation for the flames for hydrogen fuel and hydrogen hydrocarbon blended fuels [30].

For $CH^*(A)$ formation, four reactions were proposed by Smith *et al.* [28]:

$$C_2H+O_2=CH^*+CO_2 \quad (R3)$$
$$C_2H+O=CH^*+CO \quad (R4)$$
$$C_2+OH=CH^*+CO \quad (R5)$$
$$C+H+M=CH^*+M \quad (R6)$$

The reactions of ethynyl radical (C_2H) with oxygen, R3 and R4, are regarded as the dominating pathway by several researchers [32-36]. The $CH^*(A)$ formation pathway from C_2 (R5) was suggested by Gaydon [37] however, according to the recent investigation of Smith *et al.* [28], R5 plays only a minor role in methane flames. R6 was first proposed by Smith *et al.* [28] and its rate constant is estimated from R2.

For the C_2^* Swan band chemiluminescence formation reactions, less attention has been paid to these CH_2+C pathway (R6) was firstly suggested by Bowman *et al.* [38] and further supported by Grebe and Homann [39] in a flow discharge examination of kinetics in the C_2H_2/O/H system. Another pathway of C_2^* formation (R7) is through C_3 reaction with oxygen, as suggested by Savadatti and Broida [40] in carbon vapour flames in oxygen.

$$CH_2+C=C_2^*+H_2 \quad (R6)$$
$$C_3+O=C_2^*+CO \quad (R7)$$

For CO_2^* chemiluminescence, the only available detailed formation mechanism, R8 and R9, was proposed by Kopp *et al.* [41, 42] with the shock tube measurement in the $H_2/N_2O/CO/Ar$ system. This CO_2^* chemiluminescence mechanism was examined in the n-Heptane diesel engine condition, however, and only fair agreement was achieved with the experimental result in the optical engine.

$$CO+O+M=CO_2^*+M \quad (R8)$$
$$HCO+O=CO_2^*+H \quad (R9)$$

In the present investigation, the chemiluminescence of OH^*, $CH^*(A)$, C_2^* and CO_2^* were simultaneously simulated in non-preheated (T_{in} = 300 K) counterflow flames under atmosphere pressure conditions. The flames' equivalence ratios (ER) ranged from 0.6 to 1.3, and strain rates range from 80 s^{-1} to 400 s^{-1}, were considered to examine the correlation between chemiluminescence and

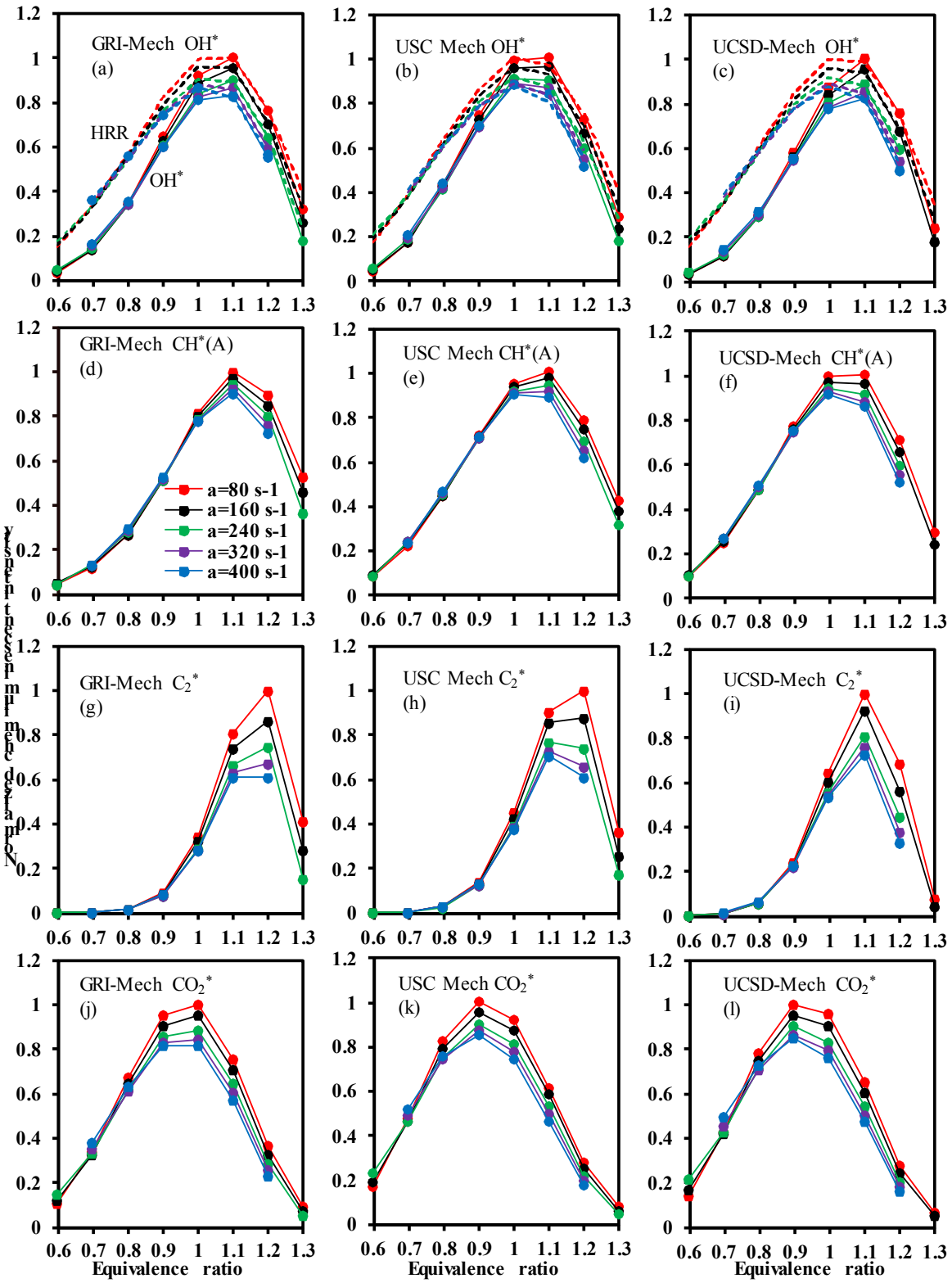

Figure 1 Normalized OH*, CH*(A), C_2* and CO_2* chemiluminescent intensity and heat release rate as a function of equivalence ratio and having the strain rate (a) as a parameter. The solid lines with dot represent the chemiluminescent intensity and the dash lines represent the heat release rate. (a), (d), (g), (j): results for GRI-Mech 3.0 case; (b), (e), (h), (k): results for USC Mech Version II case; (c), (f), (i), (l): results for UCSD-Mech

equivalence ratio, heat release rate and NO emission. Three widely used detailed C1-C3 mechanisms, GRI-Mech 3.0 [43], that due to USC Mech Version II [44] and The UCSD-Mech [45], were coupled with the chemiluminescence mechanism to assess the thermal mechanism effect on the chemiluminescence.

Chemical Mechanism

The employed OH^*, $CH^*(A)$ and C_2^* chemiluminescence mechanism was modified based on the one adopted by Kathrotia *et al.*[29, 46]. The reaction rate of the OH^* chemiluminescence formation path from hydrocarbon (R2) was updated according to the recent shock-tube measurement by Bozkurt and Metehan [47]. The CO_2^* chemiluminescence model proposed by Kopp *et al.*[41, 42] was employed. Because C_2, C_2H and C_3 are included in R3, R4, R5 and R7, elementary reactions for C, C2 and C3 species were added in the fuel oxidant mechanism: these elementary reactions were same as the reactions used in Kathrotia *et al.*[29, 46]. The thermochemical data from Burcat–Ruscic thermochemical database [48] was employed for the excited species and for the C, C2 and C3 species. The transport coefficients data were from the fuel oxidant mechanisms. The NO mechanism was provided by GRI-Mech 3.0 [43].

Numerical Conditions

The OPPDIF code [49] was employed to simulate the 1-D premixed counterflow flames. The results were obtained for the equivalence ratio range of 0.6 to 1.3 and strain rate range from 80 to 400 s^{-1} corresponding to the air-fuel mixture's bulk velocity at the nozzle exit V=1-5m/s. The pressure and temperature of the fuel-air mixture were set at 1 bar and 300K respectively. The transport coefficients were calculated using mixture-averaged formulation.

The absolute tolerance and relative tolerance for iteration and time stepping were 1E-13 and 1E-6 respectively. The convection terms were discretized by upwind scheme. To ensure the accuracy of the calculated heat release rate and chemiluminescent intensity peak position, a very fine mesh was used. The final mesh had approximate 400 to 800 points, depending on the main oxidant mechanism.

Results and Discussion

To assess the ability of chemiluminescence from different excited species in indicating HRR, and to further understand the oxidant mechanism effect on predicting chemiluminescence, a comparison between the HRR and chemiluminescent intensities from different excited species is necessary. Figure 1 plots the normalized OH^*, $CH^*(A)$, C_2^* and CO_2^* chemiluminescent intensity and HRR a function of equivalence ratio and having the strain rate as a parameter. The chemiluminescent intensity and HRR are calculated in premixed methane-air flame, based on the three different fuel oxidant mechanisms as discussed previously. The calculated OH^* chemiluminescent intensity based on GRI-Mech 3.0 increased monotonically with ER for all values of strain rate for $0.6 < ER < 1.1$, and decreased monotonically with increasing ER thereafter. According to the results calculated in the present study, the strain rate did not seem to have an effect on the heat release rate or the chemiluminescent intensity for the lean flames, but there was a strain rate effect on the both calculated quantities for the ER >0.9 flames, shown in Figure 1 (a). In contrast, the experimental results showed that there was an effect of the strain rate for all the range of ER studied [50]. Figure 1 (b) and (c) illustrate the calculated OH^* chemiluminescent intensity based on Mech Version II and UCSD-Mech. No significant difference was found among these three calculated OH^* chemiluminescent intensities. For all three calculated OH^* chemiluminescent intensities, the maximum values were achieved at ER=1.1, which is very close to the equivalence ratio of peak HRR. Figure 1 (d), (e) and (f) show the predicted $CH^*(A)$ chemiluminescent intensity. The behaviors of $CH^*(A)$ as a function of equivalence ratio and strain rate were similar to OH^*. The $CH^*(A)$

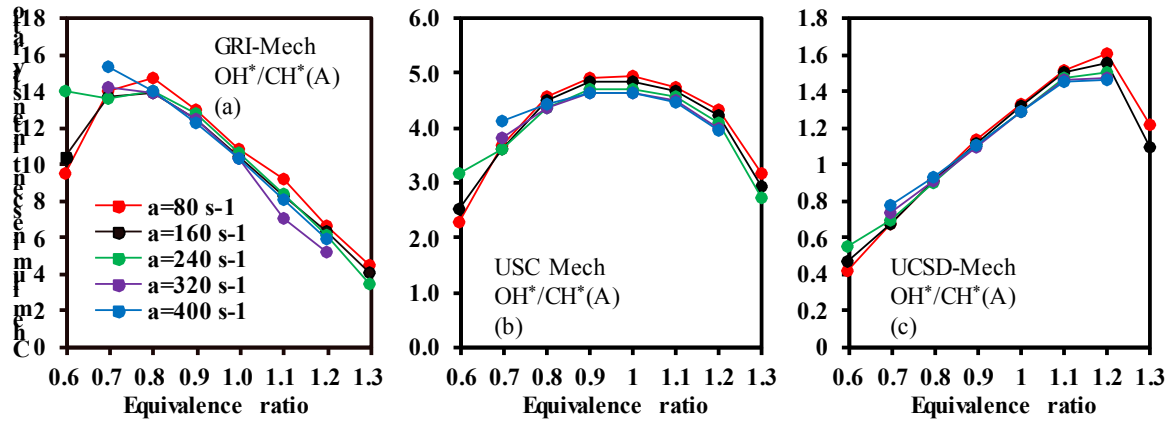

Figure 2 Calculated $OH^*/CH^*(A)$ chemiluminescent intensity ratio as a function of equivalence ratio having the strain rate as parameter. (a): results for GRI-Mech 3.0 case; (b) results for USC Mech Version II case; (c): results for UCSD-Mech case.

chemiluminescent intensity increased with equivalence ratio from 0.6 to 1.1 and monotonically decreased thereafter. However, the peak CH^*(A) chemiluminescent intensity predicted by UCSD-Mech occurred at ER=1.0 while, for the other two cases, the peak CH^*(A) chemiluminescent intensities occurred at ER=1.1. For the C_2^* chemiluminescent intensity, a substantial difference between these three predicted results were exists, see Figure 1 (g), (h) and (i). For the GRI-Mech 3.0 case, the peak intensity of C_2^* was found at ER=1.2, and the strain rate did not influence the ER of peak C_2^* chemiluminescent intensity: these phenomena agree with our previous published experimental results [50]. However, for the USC Mech Version II case, the ER of peak C_2^* chemiluminescent intensity occurred at 1.2 for the cases with strain rates lower than 160 s^{-1}, while, with the strain rate increased, the peak C_2^* moved to ER=1.1 for the cases with strain rate of 240, 320 and 400 s^{-1}. And in the UCSD-Mech cases, all the C_2^* chemiluminescent intensity reached peak values at ER=1.1. For the CO_2^* chemiluminescent intensities, the variation for difference ER and strain rates are plotted in Figure 1 (j), (k) and (l). The behavior of CO_2^* variation with ER were similar to OH^*. The strain rate effect was minor but more notable than that on OH^*; the CO_2^* chemiluminescent intensities were generally dominated by stoichiometry. Differences can be found between GRI-Mech 3.0 and other two mechanisms. The peak CO_2^* chemiluminescent intensities predicted by the GRI-Mech 3.0 mechanism occurred at ER=1.0 for all the strain rates, while, for other two cases, the peak CO_2^* occurred at ER=0.9. Compared with previous experimental results[50], the calculated CO_2^* chemiluminescent intensities based on GRI-Mech 3.0 were the closer.

The chemiluminescent intensity ratio of OH^* and CH^*(A) has been suggested as an equivalence ratio marker by many researchers: however, the fuel oxidant mechanism effect on predicting this ratio has not been examined previously. Figure 2 illustrates the calculated OH^*/CH^*(A) chemiluminescent intensity ratio for the three different fuel oxidant mechanisms. For the GRI-Mech 3.0 case, the calculated OH^*/CH^*(A) chemiluminescent intensity ratios was monotonically increased in equivalence range from 0.6 to 0.8 and decreased from 0.8 to1.3 for strain rates lower 160 s^{-1}. For the higher strain rate cases, strain rate above 240 s^{-1}, the OH^*/CH^*(A) chemiluminescent intensity ratio monotonically decreases with increase in equivalence ratio. Nevertheless, for all these cases, the effect of strain rate was minor when compared with the equivalence ratio effect. The predicted $OH^*/CH(A)^*$ chemiluminescent intensity ratios, based on GRI-Mech 3.0, generally achieved very good qualitative and quantitatively agreements with measured results [15, 21, 50, 51]. However, for the Mech Version II case, the maximum of OH/CH^*(A) chemiluminescent

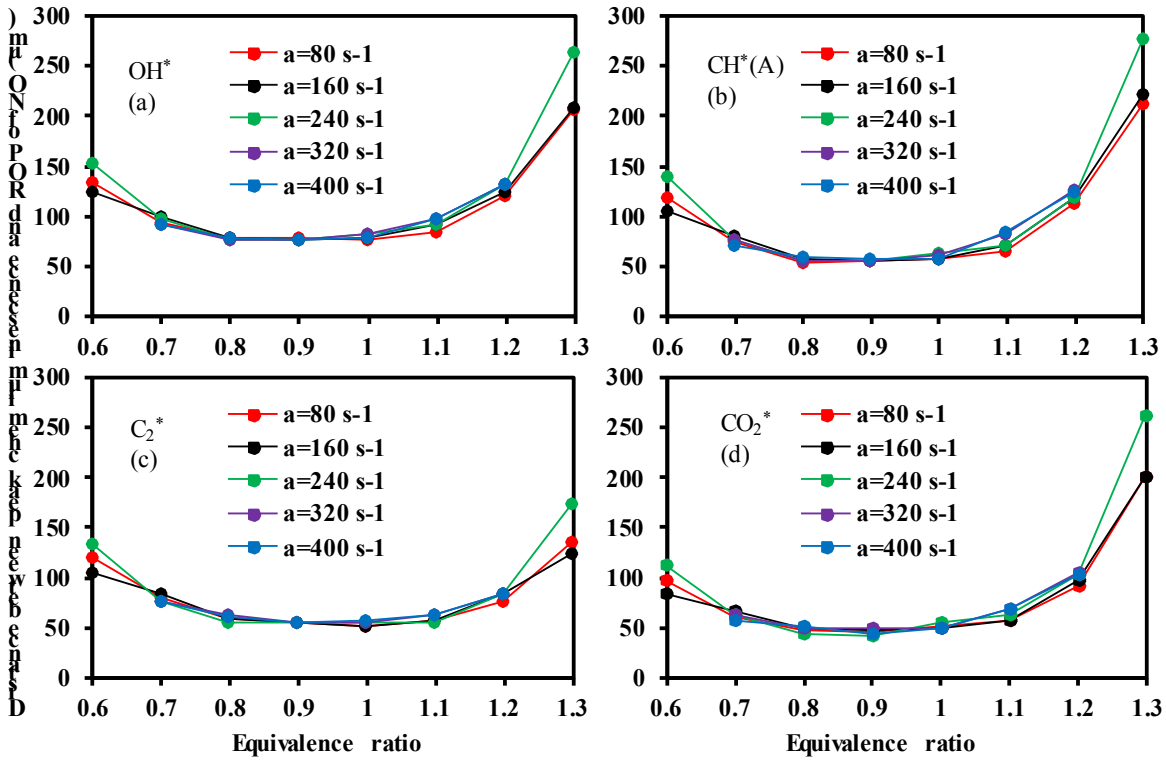

Figure 3 Distance between peak chemiluminescence and peak production rate of NO in methane-air flames plotted against equivalence ratio and having strain rate as parameter. (a): peak to peak distance between OH^* and rate of production (ROP) of NO; (b): peak to peak distance between CH^*(A) and ROP of NO; (C): peak to peak distance between C_2^* and ROP of NO; (d): peak to peak distance between CO_2^* and ROP of NO.

intensity ratios occurred at ER between 0.9 to 1.0, depending on the strain rate. Moreover, for the UCSD-Mech, the trend of $OH/CH^*(A)$ chemiluminescent intensity ratio behaviour was in reverse to the GRI-Mech 3.0 case: the $OH/CH^*(A)$ increased with ER in range from 0.6 to 1.2 and then decreased at ER=1.3. As far as quantitative results are concerned, the magnitude of $OH/CH^*(A)$ chemiluminescent intensity ratio predicted based on Mech Version II fuel oxidant mechanism was about half of the magnitude predicted based on GRI-Mech 3.0. Moreover, the $OH^*/CH^*(A)$ chemiluminescent intensity ratios for UCSD-Mech cases were approximately one tenth of the GRI-Mech 3.0 cases. These phenomena suggest that the main fuel oxidant mechanism influences not only the magnitude of $OH^*/CH^*(A)$ chemiluminescent intensity ratio but also its tendency.

Chemiluminescence has been used for online monitoring of NO emission for combustor control [52]. To examine the relationship between chemiluminescence and NO production, the distance between peak chemiluminescence and NO rate of production (ROP) is plotted in Figure 3. Generally, for the lean flames, the peak to peak distances between chemiluminescence and NO ROP were less than 100 μm, especially for the CO_2^* and C_2^* chemiluminescence, shown in Figure 3 (d). Moreover, both the strain rate and equivalence ratio did not significantly influence this peak to peak distance except for the cases at ER=1.3 and ER=0.6.

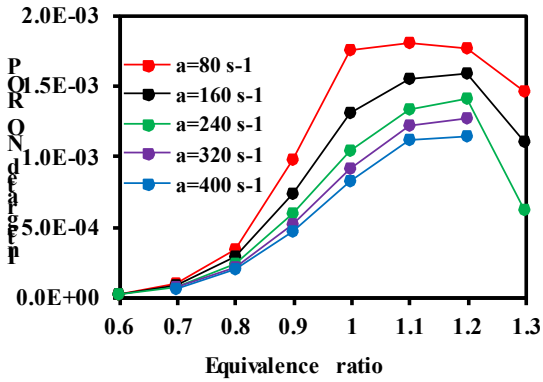

Figure 4 The calculated overall NO ROP for the flame area plotted against equivalence ratio.

To further understand the relation between NO emission and chemiluminescence, the calculated overall NO ROP for the flame area is shown in Figure 4. The overall NO ROP increased with equivalence ratio in the lean flames and was highest at between ER=1.1 to 1.2, depending on the strain rate. Both the equivalence ratio and strain rate effect are significant. Thus, a combination of C_2^* and CO_2^* can correlate with the NO ROP behaviour. Leaner than ER=0.9, the CO_2^* chemiluminescence behaviours follow the trend of NO ROP. Richer than ER=0.9, the C_2^* is the more reliable indicator and shows the highest magnitude at ER=1.2. Moreover, the combination of CO_2^* and C_2^* is convenient in practice because the wavelength of the C_2^* Swan band overlaps with the wavelength of CO_2^*. Because photomultiplier based measurements cannot distinguish CO_2^* and C_2^* chemiluminescence, the measurement of C_2^* chemiluminescent intensity based on the photomultiplier signal can be treated as the total intensity of CO_2^* and C_2^* chemiluminescence. The combination result of CO_2^* and C_2^* measurement can be found in Figure3 of [50], the measured combined CO_2^* and C_2^* chemiluminescent intensity follows the NO ROP trend very well.

Conclusions

- The fuel oxidant mechanism is important for predicting chemiluminescent intensities and their ratio. A good combination of fuel oxidant mechanism and chemiluminescence mechanism can qualitatively and quantitatively reproduce the experimental results.
- The OH^*, $CH^*(A)$ and CO_2^* chemiluminescent intensity can be utilized to indicate HRR behaviour; the $OH^*/CH^*(A)$ chemiluminescent ratio is capable of marking the equivalence ratio.
- The CO_2^* and C_2^* chemiluminescence are able to indicate the NO ROP position in the evaluated flame and the combined CO_2^* and C_2^* chemiluminescent intensity can follow the NO ROP behaviour very well. This combination is easy to achieve in practice.

Acknowledgements

The authors would like to acknowledge the support of Engineering and Physical Research Council (EPSRC) through grant EP/K021095/1 "Flexible and Efficient Power Plant (Flex-E-Plant)" and the financial support of the China Scholarship Council (CSC).

References

1. C. Oh; A. Hamins; M. Bundy; J. Park, Combustion Theory and Modelling 12 (2) (2008) 283-302
2. G. Coppola; B. Coriton; A. Gomez, Combustion and Flame 156 (9) (2009) 1834-1843
3. L. Kostiuk; K. Bray; R. Cheng, Combustion and flame 92 (4) (1993) 396-409
4. C. M. Vagelopoulos; F. N. Egolfopoulos, in: *Symposium (International) on Combustion*, 1994; Vol. 25, pp 1317-1323.
5. G. Jomaas; X. Zheng; D. Zhu; C. Law, Proceedings of the Combustion Institute 30 (1) (2005) 193-200
6. E. Mastorakos; A. Taylor; J. Whitelaw, Combustion and Flame 102 (1) (1995) 101-114
7. O. Gicquel; N. Darabiha; D. Thévenin, Proceedings of the Combustion Institute 28 (2) (2000) 1901-1908 http://dx.doi.org/10.1016/S0082-0784(00)80594-9.
8. G. S. Jackson; R. Sai; J. M. Plaia; C. M. Boggs; K. T. Kiger, Combustion and Flame 132 (3) (2003) 503-511
9. K. K. Venkatesan; G. B. King; N. M. Laurendeau; M. W. Renfro; B. Böhm, Flow, turbulence and combustion 83 (1) (2009) 131-152

10. H. Guo; G. J. Smallwood; F. Liu; Y. Ju; Ö. L. Gülder, Proceedings of the combustion institute 30 (1) (2005) 303-311
11. M. Nishioka; S. Nakagawa; Y. Ishikawa; T. Takeno, Combustion and Flame 98 (1–2) (1994) 127-138 http://dx.doi.org/10.1016/0010-2180(94)90203-8.
12. E.-S. Cho; S. H. Chung, Journal of mechanical science and technology 23 (3) (2009) 659-666
13. M. C. Drake; R. J. Blint, Combustion science and technology 75 (4-6) (1991) 261-285
14. J. Floyd; P. Geipel; A. Kempf, Combustion and Flame 158 (2) (2011) 376-391
15. Y. Hardalupas; M. Orain, Combustion and Flame 139 (3) (2004) 188-207 http://dx.doi.org/10.1016/j.combustflame.2004.08.003.
16. Y. Hardalupas; C. Panoutsos; A. Taylor, Experiments in fluids 49 (4) (2010) 883-909
17. M. Orain; Y. Hardalupas, Comptes Rendus Mécanique 338 (5) (2010) 241-254 http://dx.doi.org/10.1016/j.crme.2010.05.002.
18. J.-M. Samaniego; F. Egolfopoulos; C. Bowman, Combustion Science and Technology 109 (1-6) (1995) 183-203 Doi 10.1080/00102209508951901.
19. T. Muruganandam; B. Kim; R. Olsen; M. Patel; B. Romig; J. Seitzman, AIAA paper 4490 (2003)
20. C. S. Panoutsos; Y. Hardalupas; A. M. K. P. Taylor, Combustion and Flame 156 (2) (2009) 273-291 http://dx.doi.org/10.1016/j.combustflame.2008.11.008.
21. J. Kojima; Y. Ikeda; T. Nakajima, Proceedings of the Combustion Institute 28 (2) (2000) 1757-1764 http://dx.doi.org/10.1016/S0082-0784(00)80577-9.
22. Y. Ikeda; J. Kojima; H. Hashimoto, Proceedings of the Combustion Institute 29 (2) (2002) 1495-1501 Doi 10.1016/S1540-7489(02)80183-3.
23. T.-S. Cheng; C.-Y. Wu; Y.-H. Li; Y.-C. Chao, Combustion science and technology 178 (10-11) (2006) 1821-1841 10.1080/00102200600790755.
24. T. García-Armingol; J. Ballester, International Journal of Hydrogen Energy 39 (35) (2014) 20255-20265 http://dx.doi.org/10.1016/j.ijhydene.2014.10.039.
25. J. Kojima; Y. Ikeda; T. Nakajima, Measurement Science and Technology 14 (9) (2003) 1714 Pii S0957-0233(03)61877-1
Doi 10.1088/0957-0233/14/9/324.
26. Y. Hardalupas; M. Orain; C. S. Panoutsos; A. Taylor; J. Olofsson; H. Seyfried; M. Richter; J. Hult; M. Aldén; F. Hermann, Applied thermal engineering 24 (11) (2004) 1619-1632 10.1016/j.applthermaleng.2003.10.028.
27. N. Docquier; F. Lacas; S. Candel, Proceedings of the Combustion Institute 29 (1) (2002) 139-145 Doi 10.1016/S1540-7489(02)80022-0.
28. G. P. Smith; J. Luque; C. Park; J. B. Jeffries; D. R. Crosley, Combustion and Flame 131 (1) (2002) 59-69 Pii S0010-2180(02)00399-1
Doi 10.1016/S0010-2180(02)00399-1.
29. T. Kathrotia; U. Riedel; A. Seipel; K. Moshammer; A. Brockhinke, Applied Physics B 107 (3) (2012) 571-584 10.1007/s00340-012-5002-0.
30. T. Kathrotia; M. Fikri; M. Bozkurt; M. Hartmann; U. Riedel; C. Schulz, Combustion and Flame 157 (7) (2010) 1261-1273
31. T. Kathrotia, (2011)
32. G. Glass; G. Kistiakowsky; J. Michael; H. Niki, The Journal of Chemical Physics 42 (2) (1965) 608-621
33. M. Bozkurt; M. Fikri; C. Schulz, Applied Physics B 107 (3) (2012) 515-527
34. R. M. Elsamra; S. Vranckx; S. A. Carl, The Journal of Physical Chemistry A 109 (45) (2005) 10287-10293
35. A. Renlund; F. Shokoohi; H. Reisler; C. Wittig, Chemical Physics Letters 84 (2) (1981) 293-298
36. S. Hwang; W. Gardiner; M. Frenklach; Y. Hidaka, Combustion and flame 67 (1) (1987) 65-75
37. A. G. Gaydon, The spectroscopy of flames, 1957, p.^pp.
38. C. T. Bowman; D. J. Seery, Combustion and Flame 12 (6) (1968) 611-614
39. J. Grebe; K. Homann, Berichte der Bunsengesellschaft für physikalische Chemie 86 (7) (1982) 587-597
40. M. Savadatti; H. Broida, The Journal of Chemical Physics 45 (7) (1966) 2390-2396
41. M. Kopp; M. Brower; O. Mathieu; E. Petersen; F. Güthe, Applied Physics B 107 (3) (2012) 529-538 10.1007/s00340-012-5051-4.
42. M. M. Kopp; O. Mathieu; E. L. Petersen, International Journal of Chemical Kinetics 47 (1) (2015) 50-72
43. G. P. Smith; D. M. Golden; M. Frenklach; N. W. Moriarty; B. Eiteneer; M. Goldenberg; C. T. Bowman; R. K. Hanson; S. Song; W. C. Gardiner Jr, in: *URL: http://www.me.berkeley.edu/gri_mech*, 1999; Vol. 51, p 55.
44. H. Wang; X. You; A. V. Joshi; S. G. Davis; A. Laskin; F. Egolfopoulos; C. K. Law, in: 2007.
45. U. Mechanism, in: *Mechanical and Aerospace Engineering (Combustion Research), University of California at San Diego (http://combustion.ucsd.edu)*, 2016.
46. T. Kathrotia; U. Riedel; J. Warnatz in: *A numerical study on the relation of OH*, CH*, and C2* chemiluminescence and heat release in premixed methane flames*, Proceedings of the European combustion Meeting, 2009; 2009; pp 1-5.
47. M. Bozkurt. Shock-tube investigation of key reactions for chemiluminescence in various combustion systems. Duisburg, Essen, Universität Duisburg-Essen, Diss., 2013, 2013.
48. A. Burcat; B. Ruscic, in: *Available from: The latest version of this database is available by anonymous FTP from ftp://ftp.technion.ac.il/pub/supported/aetdd/thermodynamics. There is a web-based mirror, http://garfield.chem.elte.hu/Burcat/burcat.html, in Europe.(2004-1997)(cited 20 December 2008)*, 2007.
49. A. E. Lutz; R. J. Kee; J. F. Grcar; F. M. Rupley, in: Sandia National Labs., Livermore, CA (United States): 1997.
50. Y. Liu; G. Vourliotakis; Y. Hardalupas; A. M. Taylor in: *Experimental and Numerical Study of Chemiluminescence Characteristics in Premixed Counterflow Flames of Methane based Fuel blends*, 55th AIAA Aerospace Sciences Meeting, 2017; 2017; p 0153.
51. N. Docquier; S. Belhalfaoui; F. Lacas; N. Darabiha; C. Rolon, Proceedings of the Combustion Institute 28 (2) (2000) 1765-1774
52. A. Cipriano; S. Gasperetti; G. Mariotti; E. Paganini in: *Analysis of the Spectral Properties of Premixed, Diffusion, and Hybrid Natural Gas Flames*, ASME Turbo Expo 2004: Power for Land, Sea, and Air, 2004; American Society of Mechanical Engineers: 2004; pp 313-320.